



Frictional stability and permeability evolution of fractures subjected to repeated cycles of heating-and-quenching: granites from the Gonghe Basin, northwest China

Li Cui · Fengshou Zhang · Mengke An ·
Li Zhuang · Derek Elsworth · Zhen Zhong

Received: 5 December 2022 / Accepted: 8 February 2023
© The Author(s) 2023

Abstract Fluid injection into enhanced geothermal system (EGS) reservoirs can reactivate subsurface fractures/faults and trigger earthquakes—requiring that frictional stability and permeability evolution characteristics are adequately evaluated. This behavior potentially becomes more complicated when the impacts of temperature and cycled thermal stresses, and the resulted damage accumulation on both stability and transport characteristics are getting involved.

We conducted coupled shear-flow experiments on saw-cut fractures recovered from an analog surface outcrop representative of a reservoir at 2450 m in the Gonghe Basin of northwestern China. The rocks were subjected to variable numbers of repeated heating-quenching (25–180–25 °C) cycles for shear-flow experiments at an effective stress of ~3 MPa and with velocity stepped between 10–1–10–1–10 μm/s. The smooth fractures return frictional coefficients in the range ~0.69 to 0.72 and are little affected by the thermal cycling. The frictional stability parameter ($a-b$) decreases and the instantaneous permeability increases with an increase in the number of heating-quenching cycles, during which intergranular and intragranular microcracks were generated in fracture surface. The above results indicate that the heating-quenching cycles during hydraulic fracturing of geothermal reservoir could affect both the fracture frictional instability and permeability evolution.

L. Cui · F. Zhang · M. An (✉)
Department of Geotechnical Engineering, College of Civil Engineering, Tongji University, Shanghai 200092, China
e-mail: 2015mengkean@tongji.edu.cn

L. Cui · F. Zhang · M. An
Key Laboratory of Geotechnical and Underground Engineering of Ministry of Education, Tongji University, Shanghai 200092, China

L. Zhuang
Korea Institute of Civil Engineering and Building Technology, Goyang, Gyeonggi 10223, Republic of Korea

D. Elsworth
Department of Energy and Mineral Engineering, EMS Energy Institute and G3 Center, The Pennsylvania State University, University Park, PA 16802, USA

D. Elsworth
Department of Geosciences, The Pennsylvania State University, University Park, PA 16802, USA

Z. Zhong
School of Civil Engineering, Shaoxing University, Shaoxing 312000, China

Article Highlights

- Heating-quenching cycles significantly affect the frictional stability of fractures in granite, although the frictional strength is relatively less affected.
- Fractures exhibit high frictional strength and a transition from v-strengthening to v-neutral behavior with increasing numbers of heating-quenching cycles.

- Instantaneous permeability increases with an increase in the number of heating-quenching cycles.
- Mineral composition affects not only the frictional strength and stability, but also the permeability evolution.

Keywords Enhanced geothermal system (EGS) · Hot dry rock · Hydraulic fracturing · Heating-quenching cycles · Permeability · Fracture stability

1 Introduction

Deep geothermal energy recovered from hot dry rock reservoirs is one of the largest, and hence most promising, geothermal resources (Barbier 2002; Moya et al. 2018; Wan et al. 2005)—with a potentially significant contribution to decarbonization of energy production (Singh et al. 2020; Watanabe et al. 2020). Enhanced geothermal systems (EGS) potentially recover heat from these ultra-low permeability reservoirs through the injection of cold-fluids to enhance permeability via creation of new fractures via thermal-shock and the reactivation of existing fractures by shear-slip (Brown et al. 2012; Wood 2009). A key issue is in defining the “Goldilocks zone” to create permeability through small-fracture reactivations with limited seismicity and avoid project terminating earthquakes (Candela et al. 2018; Lei et al. 2019a; Majer et al. 2007; Verdon and Bommer 2021). Hence, understanding the mechanisms of permeability evolution in EGS reservoirs is of great importance for the effective recovery of deep geothermal resources.

However, the injection-induced earthquakes have aroused wide public concern during deep energy extraction activities, including the enhanced geothermal systems (EGS) but also as a result of shale gas recovery, carbon dioxide (CO₂) sequestration and wastewater disposal (Atkinson et al. 2020; Bao and Eaton 2016; Clarke et al. 2019; Ellsworth 2013; Ellsworth et al. 2016). Moreover, several mid-sized and destructive earthquakes have been triggered in recent years. For example, the 2017 M_w 5.5 Pohang earthquake was one of the largest and most damaging earthquakes in South Korea over the last century—and was closely connected with the stimulation of the Pohang EGS reservoir (Chang et al. 2020; Grigoli

et al. 2018). Similarly, the Changning shale gas demonstration zone of the Sichuan basin in southwest China, has been subject to earthquakes resulting from shale gas hydraulic fracturing (e.g., the December 2018 M_L 5.7 and January 2019 M_L 5.3 earthquakes) (Lei et al. 2019b) and known to be among the largest HF-triggered events (Atkinson et al. 2020). Induced earthquakes potentially result from the hydraulic fracturing of both shale gas and EGS reservoirs, but geothermal exploitation from hot dry rock includes the impacts of sudden and extreme thermal shock (White et al. 2018). High temperature gradients in both time and space are known to damage to granite fractures (Chen et al. 2017; Peng et al. 2020) with this damage impacting the fracture/fault stability and permeability evolution (Chen et al. 2020; Zhao and Brown 1992; Zhao et al. 2020b). This heating-quenching effect on the fracture stability and permeability evolution is more pronounced in hot dry rock (granitic) reservoirs (3–5 km) at 150–250 °C than in shale reservoirs (2–3 km) at < 100 °C—and is therefore important to understand.

In recent years, laboratory experiments on the frictional stability response and permeability evolution of granite fractures have been extensively explored. This work has mainly focused on permeability evolution of natural granite fractures/faults related to hydraulic fracturing operations and the geothermal resource exploitation (Ishibashi et al. 2014; Mitchell and Faulkner 2008; Morrow et al. 2001; Watanabe et al. 2019). The results show that permeability evolution of granite fractures under hydrothermal conditions is characterized by a stress-dependent behavior and this dependence is controlled by an elastic–plastic transition of the fracture surface (Watanabe et al. 2017a). In addition, fluid injection tests have been conducted under subcritical/brittle to supercritical/ductile conditions to explore the characteristics of fluid-flow, crack propagation, and the evolution of induced permeability (Watanabe et al. 2017b). Considering that pressure dissolution on fracture surfaces could induce significant reductions in permeability through creep-closure (Caulk et al. 2016; Ishibashi et al. 2014; Shimizu 1995; Yasuhara et al. 2011, 2006; Yasuhara and Ellsworth 2004), some have questioned whether fractures could retain high permeability under long-term depletion of the reservoir (Reinsch et al. 2017). It has been demonstrated that the permeability of EGS reservoirs at very high temperatures may indeed be stabilized/

enhanced by retaining the difference between the aqueous quartz concentration and its solubility above a permeability stabilization criterion (Watanabe et al. 2020). In addition, relationships between permeability evolution and frictional strength-stability have also attracted attention (Zhang et al. 1999). The change in permeability resulting from fracture/fault slip is closely related to the lithology, fracture/fault roughness, slip distance, shear velocity and the ambient temperature and effective pressure (Blanpied et al. 1998; Passelègue et al. 2016). Thermally induced fractures and fracture/fault gouges reactivated in shear are influenced by frictional characteristics and abrupt enhancement of permeability due to the development of thermally induced cracks (Tanikawa et al. 2010). Conversely, the presence of low permeability wear products and fault gouge may result in significant reduction in permeability (Faoro et al. 2009; Moore et al. 1994; Okamoto et al. 2017; Tanikawa et al. 2014). In addition, the relationship among frictional strength, stability and permeability may also be characterized by shear-flow experiments. Results show that for granite fractures, fracture permeability is enhanced during velocity-weakening (potentially unstable) frictional slip. Two mechanisms are proposed to explain such a response, invoking changes in the fracture/fault asperity contact distribution and shear-induced dilation (Ishibashi et al. 2018). Many studies have also investigated changes in the physical-mechanical properties and damage evolution of granite under repeated heating and cooling cycles (Tang et al. 2022; Wang et al. 2020; Yin et al. 2022), but few have focused on the controlling influence of friction-stability on permeability evolution under the influence of repeated heating-quenching cycles typically observed during geothermal energy extraction.

China is rich in hot dry rock resources with the Gonghe Basin in northwestern China currently a pilot area for the demonstration of technical and economic feasibility. The thermal energy resource approaches $\sim 9.0 \times 10^{21}$ J over the depth range of 3–6 km in the Gonghe basin—equivalent to $\sim 3.1 \times 10^{11}$ t of standard coal (Zhu et al. 2015). In September 2017, the exploration well GR1 was drilled (Fig. 1a) to an in-situ temperature of 236 °C at a depth of 3705 m (Zhao et al. 2020a). In the following, we take the Gonghe geothermal reservoir as a prototype reservoir and define the frictional stability and permeability evolution of analog Gonghe

reservoir rocks subjected to repeated heating-quenching cycles and related damage accumulation. We use these results to project the response of rock fractures/faults in the Gonghe Basin for the safe and successful recovery of deep geothermal energy.

2 Experimental methods

2.1 Sample preparation

A total of seven representative core fragments (Fig. 1b) were collected from the GR1 well in the Qabqa region of the Gonghe basin (Zhang et al. 2018) at depths of 2400–3600 m. These were crushed in a ceramic mortar after removing surface impurities and sieved to a particle size $< 74 \mu\text{m}$. The mineral compositions of the seven granites were analyzed by X-ray diffraction (XRD), with the results shown in Table 1. These rocks mainly comprise quartz, plagioclase, microcline and chlorite, with traces of biotite, calcite and amphibole. The rocks are apparently altered in the interval 2900–3500 m as evident in chlorite contents in the range 25 to 39 wt.%.

The sample IDs in Table 1 index the recovered depths of the granite samples. We use local outcrops of granites for our experiments, to obviate the lack of full-size samples available from depth. The selected outcrop granite is composed of 33 wt.% quartz, 45 wt.% plagioclase, 9 wt.% biotite, 11 wt.% microcline, and 2 wt.% calcite. This outcrop granite and the seven other granites were formed at identical geological times and with mineral compositions similar to granite sample HD2450. Although dimensioning EGS reservoirs typically pays more attention to the geomechanical, deformation properties and natural fracture characteristics, the fracture frictional strength, stability and permeability evolution is mainly controlled by the fracture mineralogy (Fang et al. 2017; Ishibashi et al. 2018)—as it impacts permeability evolution in shear-flow experiments. Hence, it is reasonable to take this outcrop sample as representative of the reservoir at 2450 m (i.e. sample HD2450). From a mineralogical perspective, the differences between the outcrop sample and sample HD2450 are only the lack of minor chlorite (3 wt.%) and amphibole (3 wt.%) and the addition of minor chlorite (2 wt.%) in the outcrop sample. Such a small mineralogical difference would be expected to exert

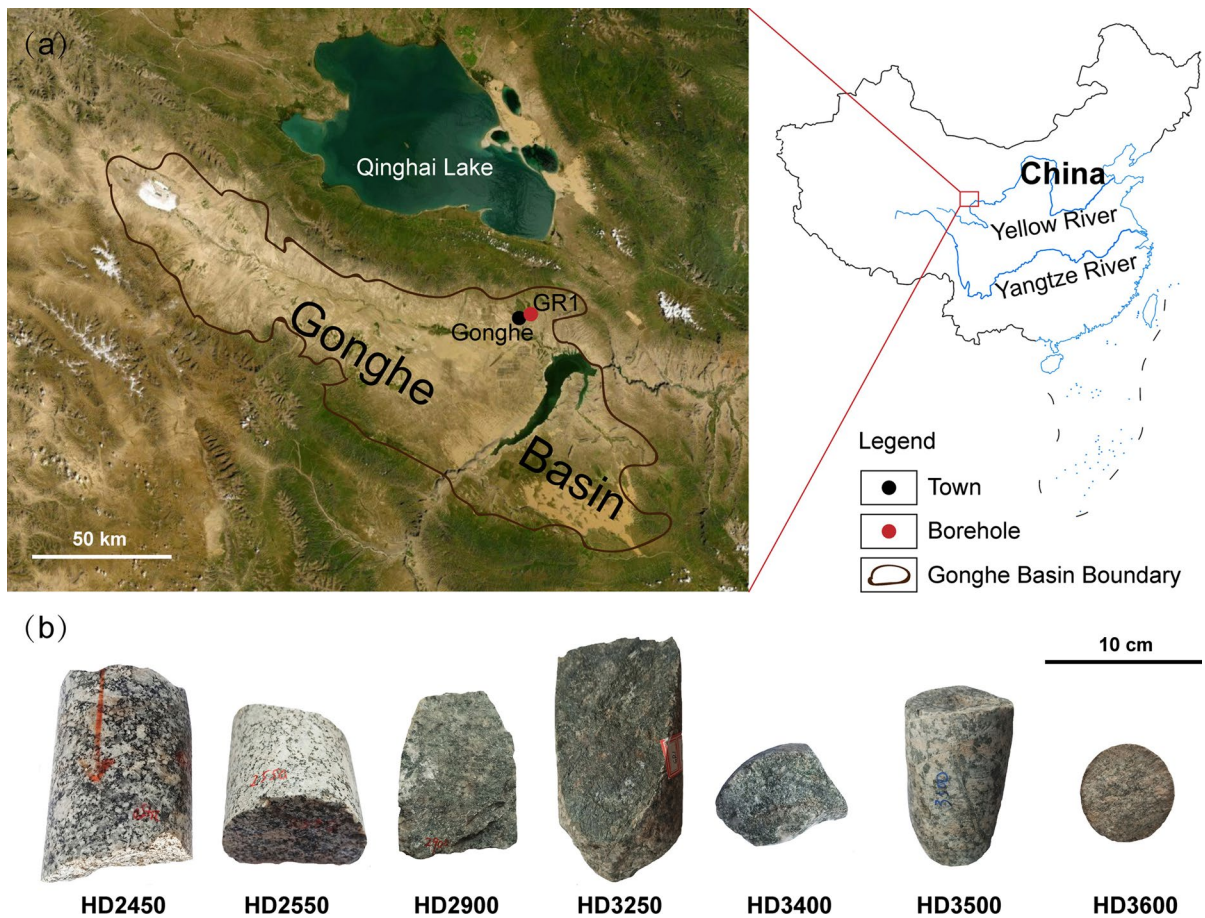


Fig. 1 **a** Location of the Gonghe basin (brown line) and injection well GR1 (red circle) in northwestern China (modified from Cao et al. 2018). The geographic coordinates of the Gonghe Basin are in the range of 98.46–101.22° E and

35.27–36.56° N. The Gonghe Basin is located to the south of the Qinghai Lake. **b** Photos of the seven cores collected from outcrop in the Gonghe basin, with most being granitic. Scale bar, 10 cm

Table 1 Mineral compositions (wt.%) with depths of the seven samples from the well GR1

Rock ID	HD2450	HD2550	HD2900	HD3250	HD3400	HD3500	HD3600
Recovered depth/m	2450	2550	2900	3250	3400	3500	3600
Quartz	32	34	39	44	39	29	32
Plagioclase	43	26	21	12	24	20	31
Microcline	8	13	12	1	5	9	21
Chlorite	3	2	25	23	29	39	11
Biotite	9	18	3	9	3	3	3
Calcite	–	–	–	11	–	–	2
Amphibole	5	7	–	–	–	–	–

only deviation of the fracture frictional properties and permeability evolution from that of the real reservoir rock.

The rock fractures are prepared according to the workflow in Fig. 2. First, cylindrical samples were drilled (diameter: 25 mm and length: 50 mm) then

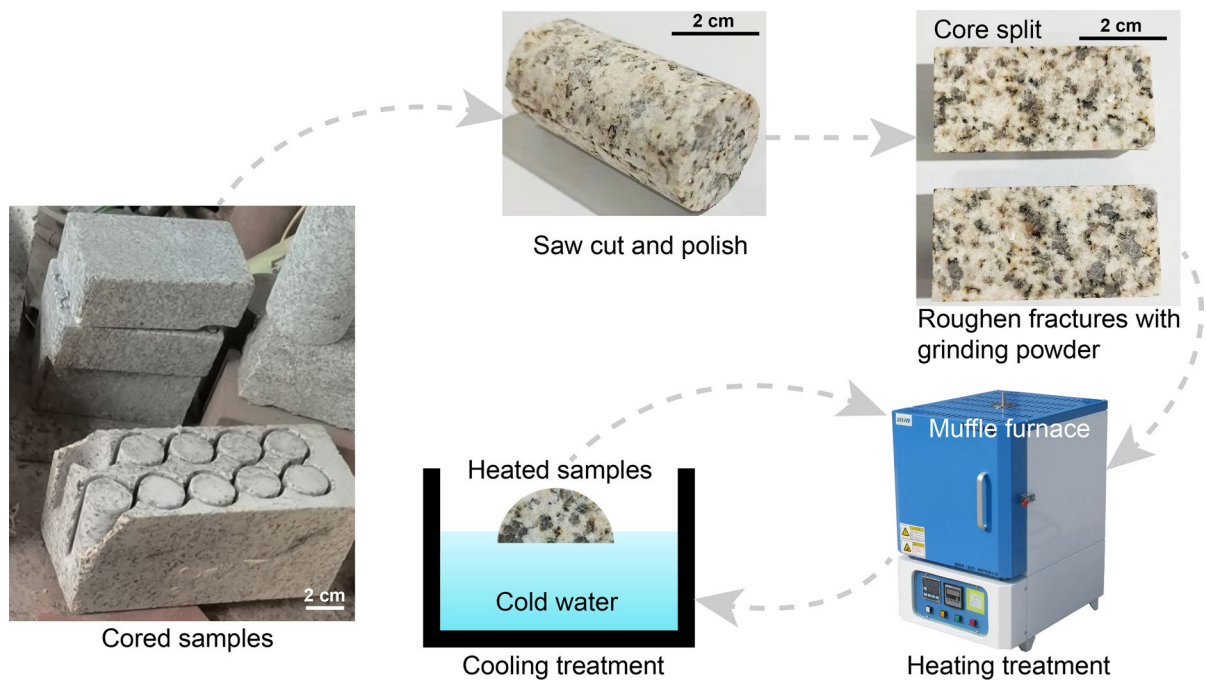


Fig. 2 Workflow for the preparation of saw-cut fractures and exposure to repeated heating-quenching cycles

polished. Then, all samples were cut along their long axis and surfaces ground with 200-mesh silicon carbide powder. Finally, the rocks were subjected to repeated heating and shock-quenching cycles in a furnace followed by removal and quenching in cold-water to simulate the cold-water injection and hot-water extraction during the recovery of deep geothermal fluids. The rock fractures were heated in a furnace (Fig. 2) to a target temperature of 180 °C, representative of the geothermal reservoir. For this, the temperature was elevated from 25 to 180 °C at a heating rate of 3 °C/min, then held constant at 180 °C for ~10 h before quenching the samples face-down in a water bath to ~25 °C. A thermocouple in the cold-water bath recorded temperature. This represented a single heating-quenching cycle.

2.2 Experimental apparatus and procedures

Shear-permeability experiments were completed in the triaxial shear-flow apparatus of the Key Laboratory of Rock Mechanics and Geohazards at Shaoxing University (Fig. 3). This apparatus can independently apply the confining pressure and the internal pore fluid pressures at a pre-defined fracture shear-offset

velocity, allowing the concurrent measurement of the evolution of fracture permeability and friction during fracture shear. The main components of the apparatus include a rock core holder, four high-precision ram pumps (pumps A, B, C and D) and experiment control and data acquisition systems (Zhong et al. 2016). The core holder accommodates both the shear of the rock fracture and concurrent water flow. When packing the sample, the split rock fractures were wrapped in Teflon tape then a latex membrane. This both seals of the rock displacing fracture and reduces membrane friction between the core and the inner jacket—reducing membrane restraint. To minimize chemical effects, we use deionized water for throughflow. Among the four ram pumps (ISCO 500D): pump A controls the confining pressure (i.e., normal stress); pumps B and C the applied shear stress/velocity, and; pump D controls the rate or pressure of the injected fluids. Each pump can effectively control the applied pressure to a resolution of ± 0.3 kPa, with the minimum flow rate of 0.001 ml/min. Shear displacement was measured and recorded by a high-precision linear variable displacement transducers (LVDT) attached to the upstream and downstream ends of the sample via the spindle of the core holder with a resolution of ± 1 μ m.

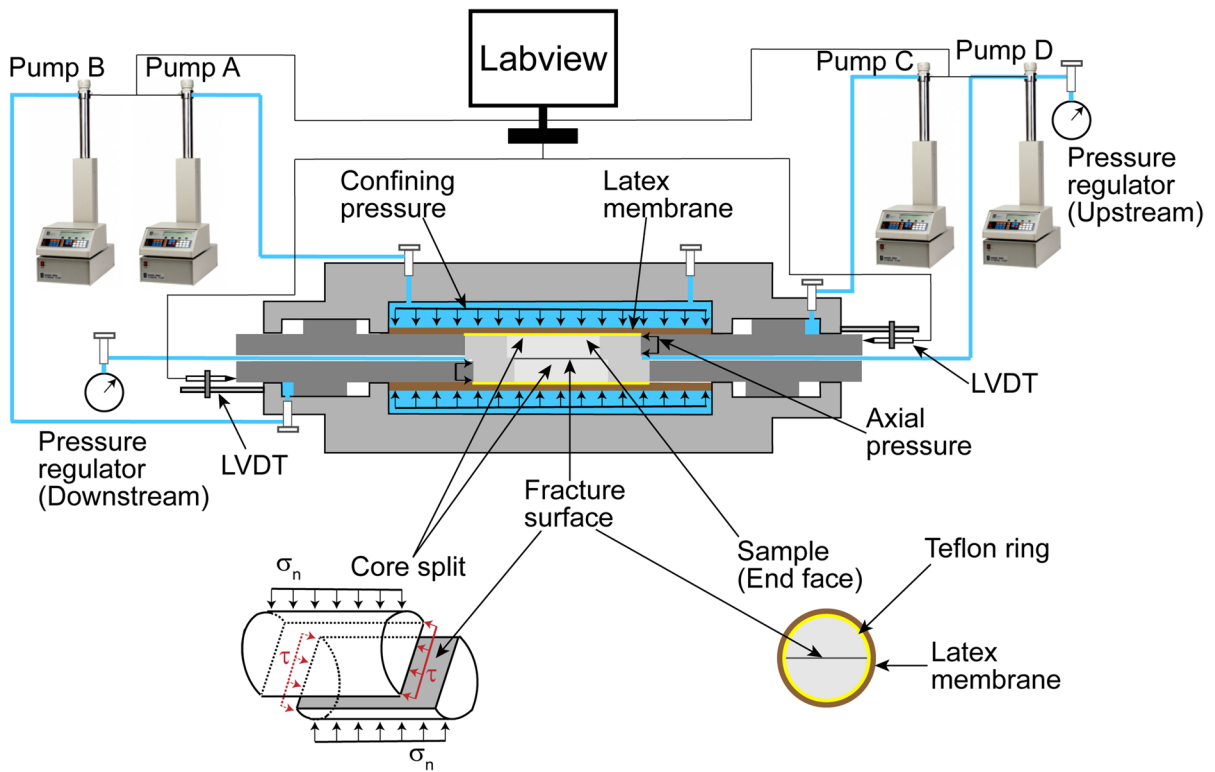


Fig. 3 Schematic of the triaxial shear-flow apparatus

The pressure difference is set to 70 kPa along the sample to allow permeability to be evaluated from the measured flow rate (pump D) and Darcy’s law. The water flow was also measured via a measuring cylinder and electronic balance at efflux. The maximum shear displacement for the rock fractures is 12 mm

with all shear experiments were carried out at a temperature of 25 °C.

To explore the impact of the number of heating-quenching cycles on the frictional stability and permeability evolution of the fractures, we performed eight shear experiments under a constant confining

Table 2 Experimental matrix of shear-flow experiments

Testing ID	Rock fractures	Heating-quenching cycles	σ_c or σ_n (MPa)	P_f (kPa)	V ($\mu\text{m/s}$)	l_{final} (mm)
SGH-0-1	SGH-1	0	3	70	10-1-10-1-10	8.13
SGH-1-1	SGH-2	1	3	70	10-1-10-1-10	7.91
SGH-3-1	SGH-3	3	3	70	10-1-10-1-10	8.21
SGH-10-1	SGH-4	10	3	70	10-1-10-1-10	8.02
SGH-30-1	SGH-5	30	3	70	10-1-10-1-10	8.03
SGH-30-2	SGH-6	30	3	70	10-1-10-1-10	8.27
SGH-30-3	SGH-7	30	3	70	10-1-10-1-10	8.14
SGH-30-4	SGH-8	30	3	70	10-1-10-1-10	8.03

σ_c = confining pressure, σ_n = normal stress, P_f = pore fluid pressure, V = shear velocity, l_{final} = final shear displacement. The confining pressure (σ_c) is equivalent to the normal stress (σ_n) for our experimental apparatus

pressure (3 MPa) and a pore fluid pressure differential of 70 kPa (Table 2). At a reservoir depth of ~2450 m, the in-situ lithostatic pressure would approach 60 MPa (considering a rock density of 2500 kg/m³) and the in-situ hydrostatic pressure would approach 25 MPa (considering a fluid density of 1000 kg/m³). Experimental shear velocities used in evaluating fracture or fault stability are generally within the range of 10⁻²–10¹ μm/s (e.g.,Blanpied et al. 1995; Moore and Lockner 2011; Tembe et al. 2010). However, it is very difficult to apply such a high confining pressure and a pore fluid pressure in our experimental apparatus. Thus, we perform our experiments at a confining pressure of 3 MPa following practical experience from previous studies (e.g., Fang et al. 2017; Ishibashi et al. 2018) and adjust the pore fluid pressure to 70 kPa to acquire the steady experimental data. Test SGH-0-1 was conducted as a control without heating-quenching cycles. Three further experiments (SGH-1-1, SGH-3-1 and SGH-10-1) were performed after 1, 3, and 10 heating-quenching cycles and a final four tests (SGH-30-1, SGH-30-2, SGH-30-3 and SGH-30-4) under identical conditions after 30 heating-quenching cycles. During the first 4-mm of shear displacement, the fractures were sheared-in at a constant shear velocity of 10 μm/s to a steady state of friction. After that, the shear-offset velocities were stepped as 10-1-10-1-10 μm/s to assess the velocity dependence of friction and stability.

2.3 Data analysis

The confining pressure, pore fluid pressure, shear stress and axial displacement were all recorded at a sampling frequency of 10 Hz. The frictional coefficient μ of the rock fracture is calculated as the ratio of the measured shear stress τ to effective normal stress σ_{neff} (ignoring the cohesion),

$$\mu = \frac{\tau}{\sigma_{neff}} = \frac{\tau}{(\sigma_n - P_f)} \tag{1}$$

where σ_n and P_f represent the applied normal stress and pore fluid pressure, respectively.

Frictional stability ($a-b$) is calculated from rate- and -state friction (RSF) law (Dieterich 1978, 1979; Marone 1998; Ruina 1983) with the coefficient of friction μ expressed as,

$$\mu = \mu_0 + a \ln \left(\frac{V}{V_0} \right) + b \ln \left(\frac{V_0 \theta}{D_c} \right) \tag{2}$$

$$\frac{d\theta}{dt} = 1 - \frac{V\theta}{D_c} \tag{3}$$

where μ is the coefficient of friction at the instantaneous shear velocity V , μ_0 is the steady-state coefficient of friction at the reference shear velocity V_0 ($V > V_0$), θ is a state variable and represents the contact age, a and b are dimensionless parameters representing the direct effect and evolutionary effect caused by the step change of shear velocity (Fig. 4b), respectively and D_c is the critical slip distance from the past steady state to a new steady state. At a steady state of friction, the state variable θ does not evolve with time and thus $d\theta/dt=0$. Then, according to Eqs. (2–3), the frictional stability ($a-b$) is defined as,

$$a - b = \frac{\mu - \mu_0}{\ln \left(\frac{V}{V_0} \right)} \tag{4}$$

Positive values of ($a-b$) indicate that the shear strength increases with an increase in shear velocity, i.e., velocity-strengthening behavior, promoting stable/aseismic fault slip. Conversely, negative values ($a-b$) indicate that the shear strength decreases with an increase in shear velocity, i.e., velocity-weakening behavior, promoting unstable/seismic fault slip whenever the critical stiffness criterion is also met (Fig. 4b).

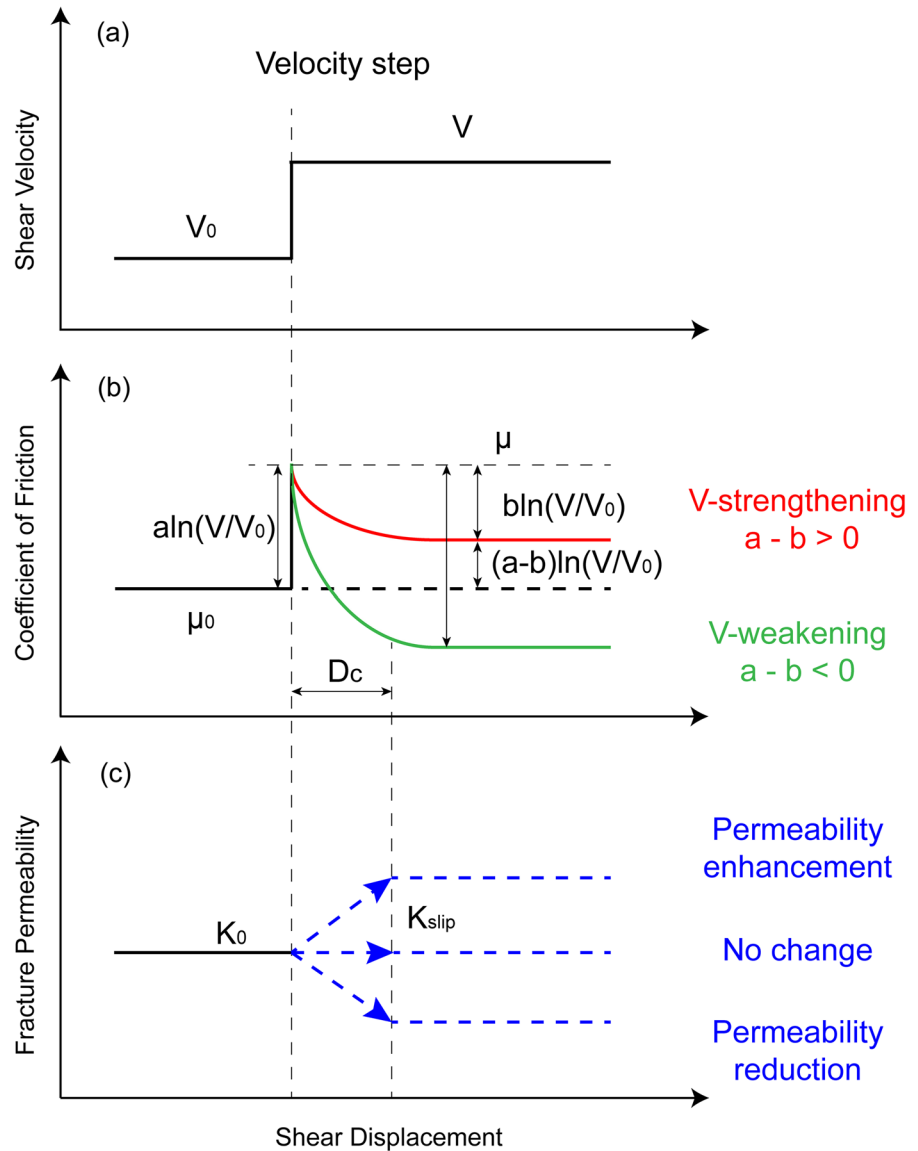
Assuming that the fracture aperture is uniform along the shear direction (Fig. 4c), the equivalent fracture permeability can be calculated based on the “cubic law”, as,

$$e_h = - \left(\frac{12\nu \cdot L \cdot Q}{W \cdot \Delta P} \right)^{1/3} \tag{5}$$

$$k = \frac{e_h^2}{12} \tag{6}$$

where e_h is the equivalent hydraulic aperture, ν is the fluid viscosity, L and W represent the fracture length and width, respectively, Q is the measured flow rate and ΔP is the fluid pressure difference between the fracture inlet and outlet. Dimensionless permeabilities

Fig. 4 Idealized representation of rate- and -state friction coupled with permeability evolution (modified from Ishibashi et al. 2018) for **a** a shear velocity-step, with associated **b** velocity-strengthening and velocity-weakening responses, and **c** related changes in permeability



are used for comparison with permeability normalized to the initial static permeability value K_0 before shear.

3 Results

3.1 Effect of heating-quenching cycles on friction of granite fracture

Following the procedures described in Sect. 2.2, eight shear-flow experiments were conducted on the multiply heated-quenched samples at $\sigma_c = 3$ MPa

and $P_f = 0.07$ MPa, with the friction-permeability-displacement curves shown in Figs. 5, 6, 7 and 8. In the first 1–2 mm of shear displacement, each sample shows a linear increase in friction and approaches the steady state following slight strain-strengthening behavior. We evaluated the steady state coefficients of friction for all fractures at a shear displacement of ~ 6.35 mm and at a shear velocity of $1 \mu\text{m/s}$. The frictional stability parameters ($a-b$) for all fractures were calculated following the methods described in Sect. 2.3. The results of coefficient of friction (μ) and frictional stability ($a-b$) are shown in Table 3 and Figs. 7 and 8.

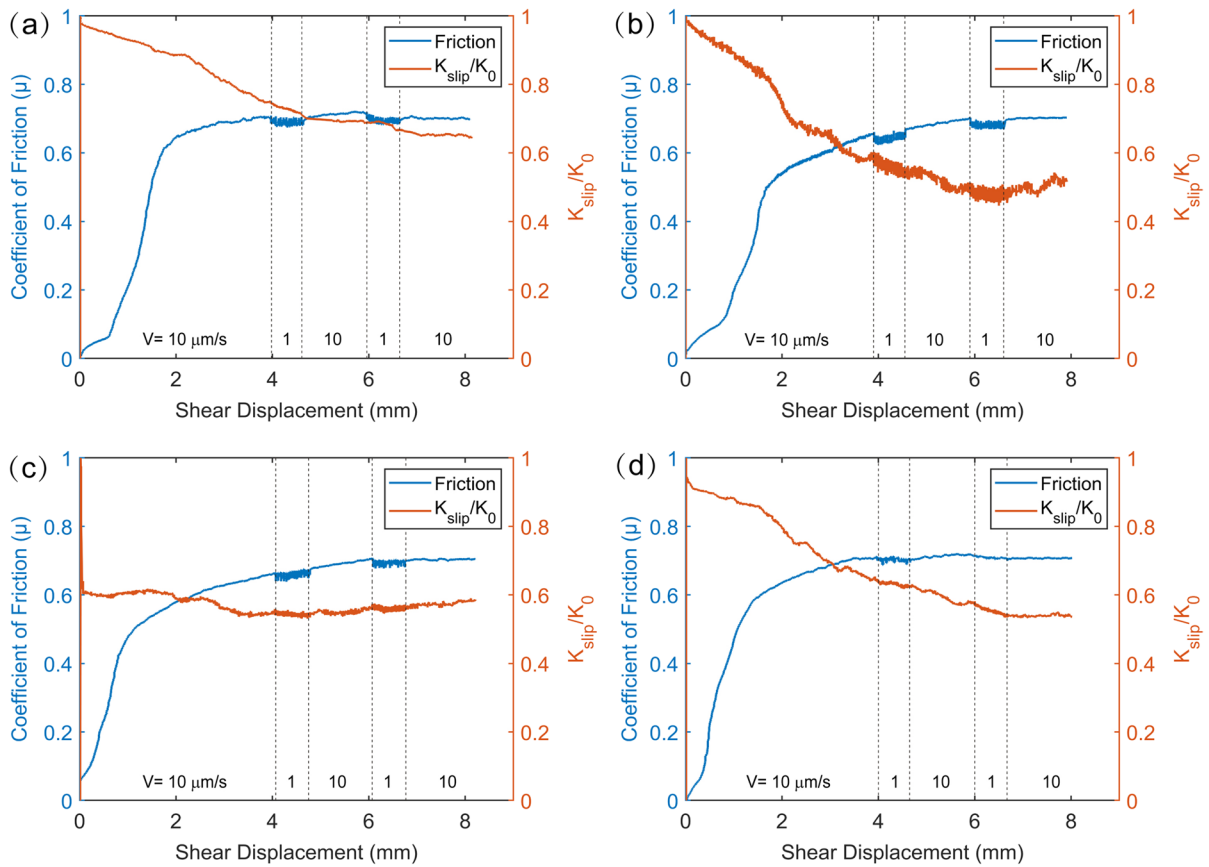


Fig. 5 Coefficient of friction (μ) and the normalized permeability (K_{slip}/K_0) versus shear displacement for tests: **a** SGH-0-1, **b** SGH-1-1, **c** SGH-3-1 and **d** SGH-10-1 for $\sigma_c=3$ MPa and $P_f=70$ kPa

The coefficients of friction μ for the eight hot dry rocks are in the range of ~ 0.69 to 0.72 , and consistent with previous results on granite fractures/faults (An et al. 2021; Sun et al. 2021). The samples are representative of the granites from well GR1 between 2450 to 3600 m where the in-situ temperatures are in the range of 180 – 230 °C. It is likely that the coefficient of friction (μ) and frictional stability ($a-b$) of these hot dry rock fractures are affected by the high temperature and cold-fluid injection during deep geothermal exploitation (Blanpied et al. 1995; Yang et al. 2022). For different heating-quenching cycles, the results show that the coefficients of friction are only slightly affected by an increase in the number of heating-quenching cycles (Figs. 7a and 8a), while the frictional stability parameters ($a-b$) are more significantly affected. Values of ($a-b$) for the eight granite fractures are in the range ~ 0.0007 to 0.0072 , indicating that these granite fractures mainly promote stable

sliding. However, the frictional stability parameters ($a-b$) decrease with an increase in the number of heating-quenching cycles (Fig. 7b). For 30 heating-quenching cycles, values of ($a-b$) for all samples are of uniform lower magnitude relative to those for fewer cycles (Fig. 8b)—suggesting a destabilizing effect of repeated heating-quenching cycles.

3.2 Effect of heating-quenching cycles on fracture permeability

To explore the effect of the number of heating-quenching cycles on permeability evolution, these eight shear experiments were monitored for flow under the uniform conditions of $\sigma_c=3$ MPa, $P_f=70$ kPa, and at ambient temperature $T=25$ °C. Normalized permeability-displacement curves are shown in earlier Figs. 5 and 6. At the initiation of the shear-flow experiment, the instantaneous permeability

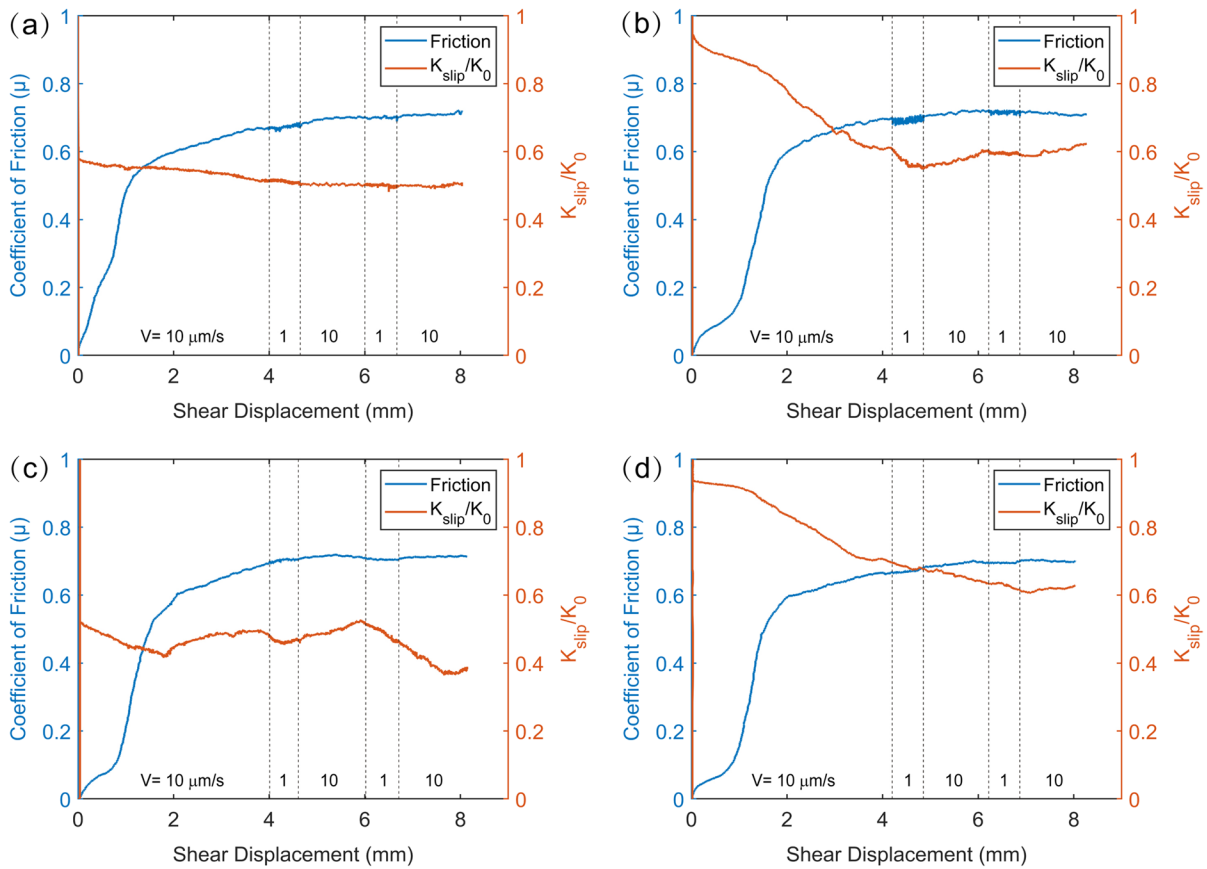


Fig. 6 Coefficient of friction (μ) and the normalized permeability (K_{slip}/K_0) versus shear displacement for tests: **a** SGH-30-1, **b** SGH-30-2, **c** SGH-30-3 and **d** SGH-30-4 for $\sigma_c = 3$ MPa and $P_f = 70$ kPa

K_{slip} first decreases by ~ 10 to 55%, followed by a gradual decrease until 4 mm shear displacement. At a shear displacement of 4–8 mm, the instantaneous permeability K_{slip} reaches a steady state and fluctuates slightly with increasing displacement, in agreement with the trend in coefficient of friction. For the control experiment (SGH-0-1) absent heating-quenching cycles (Fig. 5a), the steady-state normalized permeability of K_{slip}/K_0 is > 0.6 . With an increase in the number of heating-quenching cycles, the steady-state normalized permeability K_{slip}/K_0 decreases to 0.4–0.6 for 1, 3, and 10 heating-quenching cycles (Fig. 5b–d), and further decreases to ~ 0.4 for 30 heating-quenching cycles (Fig. 6c). These observations imply that the number of heating-quenching cycles has a slight influence on the normalized permeability evolution. We also compared the instantaneous permeability evolution with increasing shear displacement for the

eight experiments with the results shown in Fig. 9. The instantaneous permeabilities for tests SGH-0-1 (without heating-quenching cycles) and SGH-1-1 (1 heating-quenching cycle) are the lowest, followed by test SGH-3-1 (3 heating-quenching cycles). The instantaneous permeability for tests SGH-10-1 (10 heating-quenching cycles), SGH-30-1, SGH-30-2, SGH-30-3 and SGH-30-4 (30 heating-quenching cycles) are two or three times higher than those for 0–3 heating-quenching cycles. These phenomena indicate that the number of heating-quenching cycles exerts a significant impact on the instantaneous evolution of permeability.

3.3 Microstructural characterization

We explore the microstructural characteristics of four fractures subject to different numbers of

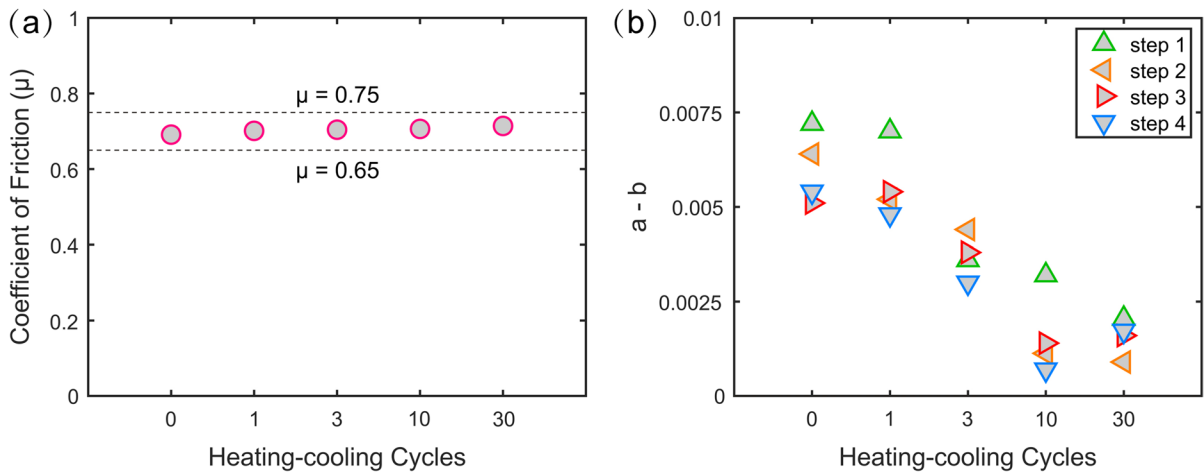


Fig. 7 Coefficient of friction (μ) and frictional stability ($a-b$) for different numbers of repeated heating-quenching cycles. The results corresponding to 30 heating-quenching cycles were the average values of tests SGH-30-1, SGH-30-2, SGH-30-3, and SGH-30-4. As the shear velocities were stepped according

to sequence “10-1-10-1-10 $\mu\text{m/s}$ ” in each test, steps 1, 2, 3 and 4 represent the shear velocity transitions of the first downstep 10–1 $\mu\text{m/s}$, then second upstep 1–10 $\mu\text{m/s}$, then third downstep 10–1 $\mu\text{m/s}$ and then fourth upstep 1–10 $\mu\text{m/s}$, respectively

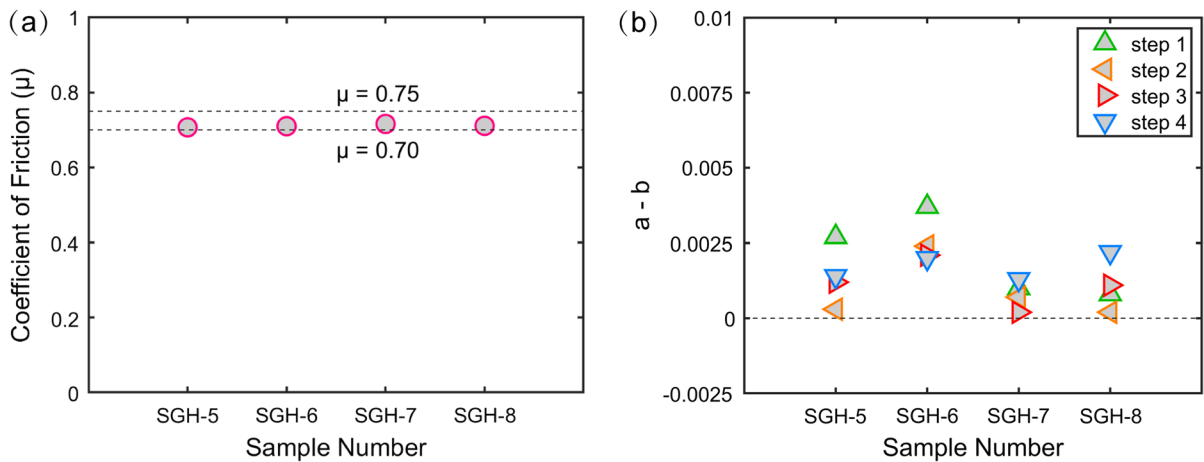


Fig. 8 Coefficient of friction (μ) and frictional stability ($a-b$) for tests SGH-30-1, SGH-30-2, SGH-30-3, and SGH-30-4. As the shear velocities were stepped according to sequence “10-1-10-1-10 $\mu\text{m/s}$ ” in each test, the steps 1, 2, 3 and 4 represent the

shear velocity transitions of the first down-step 10–1 $\mu\text{m/s}$, the second up-step 1–10 $\mu\text{m/s}$, the third down-step 10–1 $\mu\text{m/s}$ and the fourth up-step 1–10 $\mu\text{m/s}$, respectively

heating-quenching cycles (i.e., SGH-1 (without heating-quenching cycles), SGH-3 (after 3 heating-quenching cycles), SGH-4 (after 10 heating-quenching cycles) and SGH-7 (after 30 heating-quenching cycles)) (Fig. 10) for thin sections under a polarizing microscope. The control fracture SGH-1 (without heating-quenching cycles) exhibited no obvious microcracks and only several intergranular

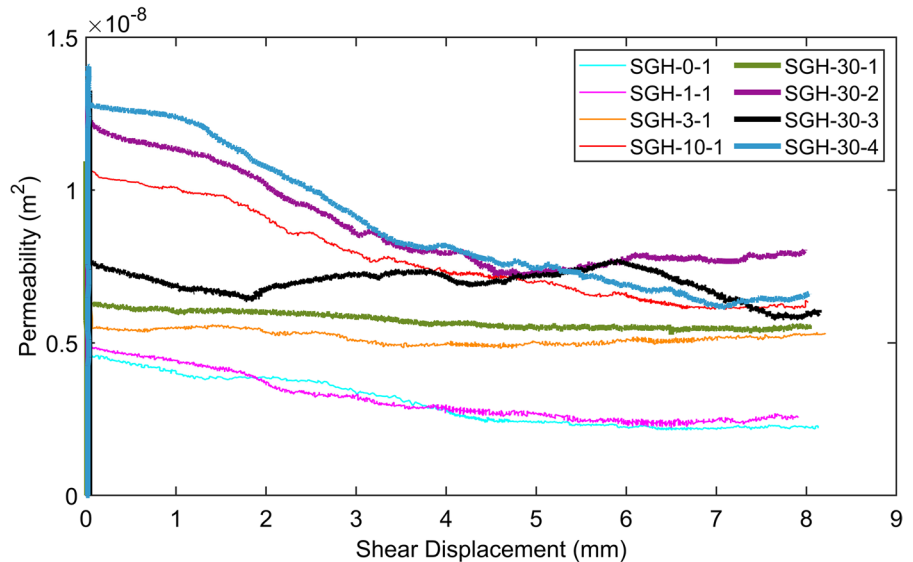
microcracks (Fig. 10a). With an increase in the number of heating-quenching cycles, more intergranular cracks developed (SGH-3 after 3 heating-quenching cycles) (Fig. 10b). Many more intergranular cracks and intragranular cracks can be observed in fractures SGH-4 and SGH-7 (Fig. 10c, d) representing 10 and 30 heating-quenching cycles. These observations suggest that numbers of repeated heating-quenching

Table 3 Coefficient of friction (μ) and calculated velocity dependence of ($a-b$) for each experiment

Testing ID	Hot dry rock fractures	μ	$(a-b)$ values at each velocity step			
			First 10–1 $\mu\text{m/s}$	Frist 1–10 $\mu\text{m/s}$	Second 10–1 $\mu\text{m/s}$	Second 1–10 $\mu\text{m/s}$
SGH-0-1	SGH-1	0.694	0.0072	0.0064	0.0051	0.0054
SGH-1-1	SGH-2	0.701	0.0070	0.0052	0.0054	0.0048
SGH-3-1	SGH-3	0.704	0.0036	0.0045	0.0038	0.0030
SGH-10-1	SGH-4	0.706	0.0032	0.0013	0.0014	0.0007
SGH-30-1	SGH-5	0.707	0.0027	0.0003	0.0012	0.0014
SGH-30-2	SGH-6	0.716	0.0037	0.0024	0.0021	0.0020
SGH-30-3	SGH-7	0.711	0.0010	0.0007	0.0020	0.0013
SGH-30-4	SGH-8	0.710	0.0008	0.0020	0.0011	0.0022

As our experiments were carried out at shear velocities of “10-1-10-1-10 $\mu\text{m/s}$ ”, the “first” and “second” indicate the sequence of the velocity step

Fig. 9 Permeability evolution with increasing shear displacement for the eight experiments under different heating-quenching cycles. Number of heating-quenching cycles denoted are noted in the serial number of experiments following “SGH” in the legend



cycles induce intense intergranular and intragranular cracks in hot dry rock fractures.

In addition, backscattered scanning electron microscope (SEM) microscopy was used to compare the microstructure of fractures both SGH-1 without heating-quenching cycles and SGH-7 after 30 heating-quenching cycles (Fig. 11). Almost no microcracks are present in the control sample SGH-1 (without heating-quenching cycles) (Fig. 11a), while intragranular microcracks across quartz crystals and intergranular microcracks between adjacent quartz and plagioclase crystals develop in fracture SGH-7 (after 30 heating-quenching cycles) (Fig. 11b)—consistent with observations under polarized light. From the

perspective of frictional stability-permeability evolution, sample SGH-1 shows clear velocity-strengthening response and is devoid of microcracks on the fracture surface, while sample SGH-7 exhibits near velocity-neutral behavior with numerous intergranular and intragranular microcracks (Fig. 11b) accompanied by clear permeability enhancement. This is consistent with previous observations (Li et al. 2021; Mo et al. 2022; Zhao et al. 2021). The transition from velocity-strengthening to velocity-weakening response is dominated by the response of strong and brittle minerals (i.e., quartz and feldspar) on the fracture surface. These brittle minerals in turn potentially impact the generation of thermally-induced

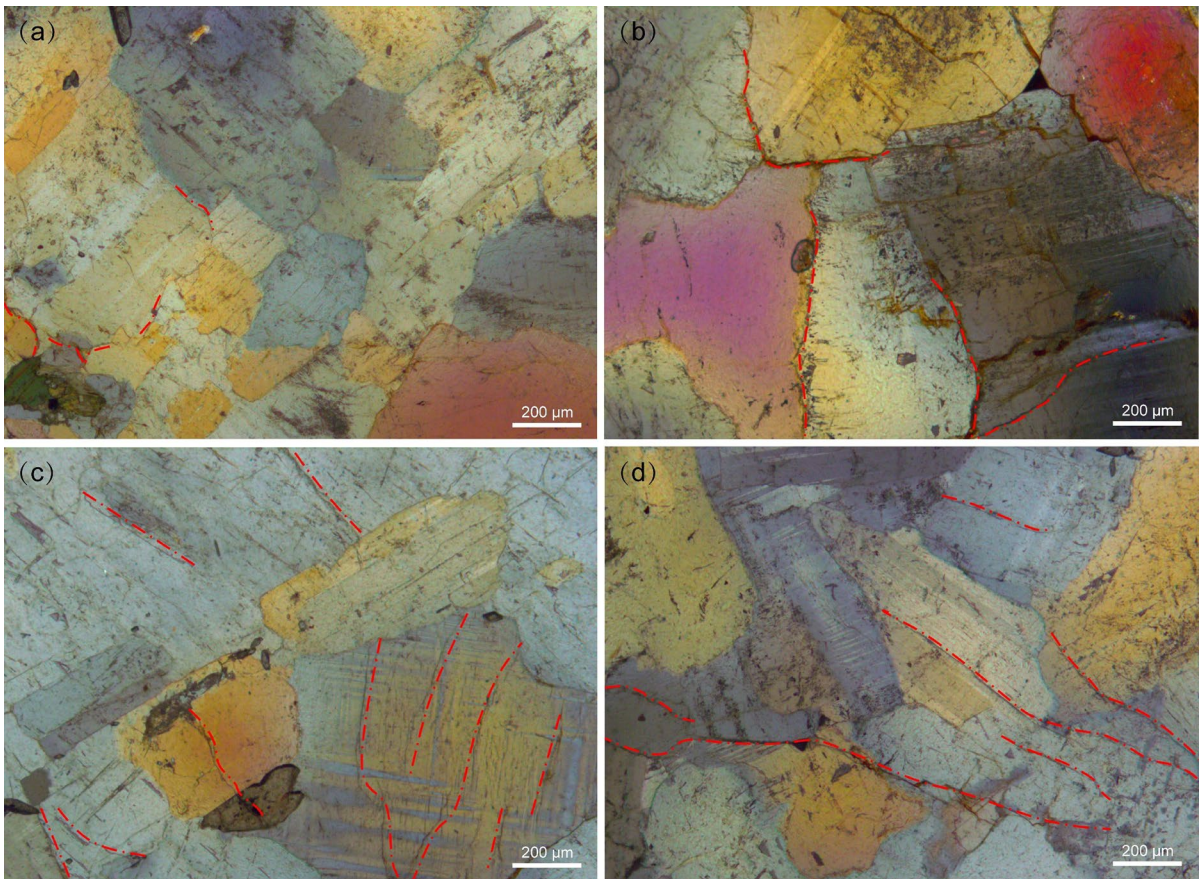


Fig. 10 Thin-section images under crossed polarized light for: **a** SGH-1 without heating-quenching cycle, **b** SGH-3 with 3 heating-quenching cycles, **c** SGH-4 with 10 heating-quenching

cycles and **d** SGH-7 with 30 heating-quenching cycles. Red dashed lines denote the observed microcracks

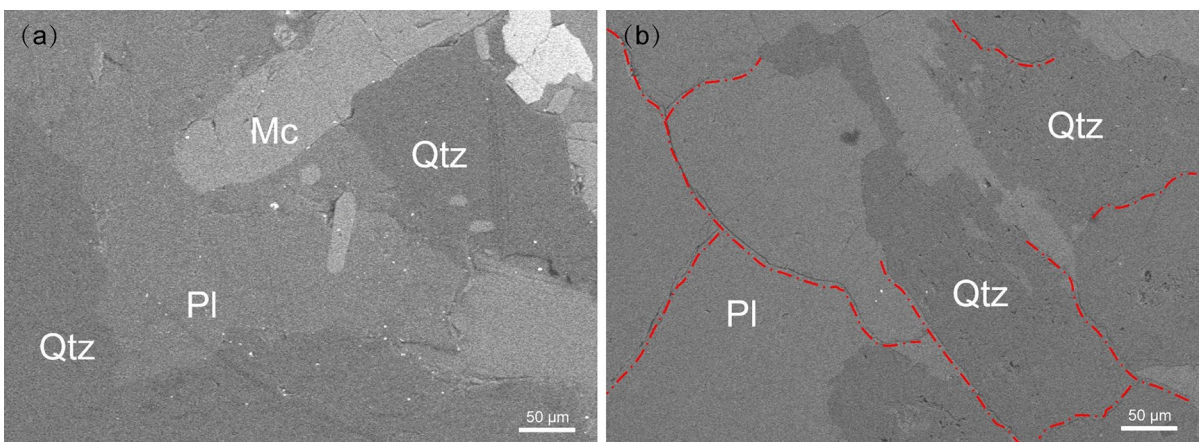


Fig. 11 Backscattered SEM (scanning electron microscope) images of fractures surfaces: **a** SGH-1 without heating-quenching cycles, and **b** SGH-7 with 30 heating-quenching cycles.

The observed microcracks are noted in red dashed lines in **b**. *Qtz* Quartz, *Pl* plagioclase, *Mc* microcline

microcracks on the fracture surface after repeated heating-quenching cycles. With an increase in the number of heating-quenching cycles, the number, length and width of the thermally-induced microcracks all increase (Weng et al. 2020; Zhang et al. 2018). Meanwhile, the form and distribution microcracking also shows a transition from an intergranular microcrack dominated to an intergranular and intragranular microcracks dominated distribution (Fig. 10).

4 Discussion

4.1 Possible mechanisms for fracture stability evolution with heating-quenching cycles

The effect of repeated heating-quenching cycles on velocity dependence of friction or friction stability ($a-b$) can be partially clarified by referring to the three different models of friction-stability-permeability evolution under low effective normal stress (Fang et al. 2017) and a microphysical model for granular gouge (den Hartog and Spiers 2014).

From Fang et al. (2017), the fracture mineral composition may exert an influence on fracture frictional strength and stability. In particular, the competition between fracture wear products and fracture expansion during shear depends on the material strength and brittleness of the fracture asperities. Strong and brittle asperities promote increased frictional strength and frictional instability relative to weak and ductile asperities. The predominant minerals in the Gonghe basin reservoir rock are of high strength and high brittleness—quartz, plagioclase and microcline. These high-strength minerals resist being broken into fine particles during shear and thus may result in the observed high frictional strength and instability.

The variation in velocity dependence of friction or frictional stability ($a-b$) can be interpreted as competition between gouge compaction caused by mineral pressure solution and shear-induced fracture dilation (den Hartog and Spiers 2014). At a low temperature and a low confining pressure, the rate of volume change is small and impact of pressure solution is not significant, and therefore deformation is dominated by the shear-induced dilation. During the

repeated heating-quenching cycles, the thermal stress induced microcracks on the fracture surface may further enhance the shear-induced dilation. This could partially account for the observed decrease in the frictional stability parameters ($a-b$) with an increase in the number of heating-quenching cycles.

4.2 Possible mechanisms for fracture permeability evolution due to heating-quenching cycles

Our results show that instantaneous fracture permeability increases with an increase in the number of heating-quenching cycles. Thermal cracking in granite typically grows more prominent with increasing temperature due to the mismatch in the thermal expansion and the anisotropy of thermal expansion in adjacent minerals (Kant et al. 2017; Wang et al. 2020; Zhang et al. 2018). When the induced thermal stress exceeds the local tensile strength, thermal cracks will occur at the boundary or across the interior of the component minerals (Jiang et al. 2018; Kumari et al. 2017). As the temperature increases, the intensity of cracking will also increase—expanding along the boundary of minerals or developing further inside minerals before finally forming penetrative cracks. Apart from the maximum temperature, the intensity of cracking is also influenced by the rate of heating in the heating-quenching cycles. Since microcracks in rock matrix will provide more channels for fluid transport, fracture permeability may also be enhanced. Additionally, an increase in the number and size of microcracks could also enhance spalling of strong brittle minerals from the fracture surface during shear. This, in turn, could promote shear dilation and further promote permeability enhancement. Consequently, the frictional instability is promoted concurrently with permeability enhancement as a result of an increased number of heating-quenching cycles. These behaviors in granite fractures significantly differ from those in shale fractures (Fang et al. 2017)—perhaps since the granites contain minor content of soft minerals in a predominantly hard and brittle matrix skeleton while shales represent the converse. This further explains that the fracture mineral compositions not only have significant effects on frictional strength and stability, but also affect the fracture permeability evolution.

4.3 Implications for geothermal energy exploitation

Our results have important implications for understanding the stability of deep faults, injection-induced seismicity and permeability evolution during geothermal energy exploitation in granitoid-hosted geothermal reservoirs. Our results imply that repeated heating-quenching cycles can induce a transition from fracture velocity-strengthening behavior to velocity-neutral behavior, potentially leading to the instability of deep faults or fractures. This evolution is beneficial for the evolution of deep geothermal reservoirs only if the instability can be restricted to small fractures, small seismic events and brittle-like porosity creation and permeability enhancement on those minor fractures. Certainly, thermal stresses promote microcracking and enhance the permeability of matrix and fractures in such reservoirs. This permeability enhancement would be beneficial for geothermal energy exploitation and also improve the efficiency of hydraulic fracturing.

As evident in previous results (Weng et al. 2020; Gautam et al. 2021), the heating-quenching cycles may create dense arrays of surface cracks and internal intergranular or intragranular microcracks. These microcracks further contribute to the degradation in rock strength, stiffness and modulus. These microcracks are induced by the accumulated tensile stresses applied around the mineral grains (such as the quartz and feldspars) and are more significant during the cooling process (Wang and Konietzky 2022; Yang et al. 2022). These results indicate that heating-quenching cycles could affect the geomechanical properties of the EGS reservoir via thermal cracking. For field application, the number of thermal cracks and crack distribution are not only dependent on the fluid injection pressure, but also affected by the number of heating-quenching cycles and the temperature difference during this cycle. Thus, the number of heating-quenching cycles and the temperature difference are both important controls on EGS reservoir fracture permeability evolution (Ishibashi et al. 2018). For induced earthquakes in EGS reservoirs, direct fluid injection may significantly reduce the effective stresses acting on deep faults and trigger the seismicity (Lee et al. 2019). From our results, the increase in number of heating-quenching cycles is shown to destabilize the granite fractures. However, this destabilization effect would be weaker in

comparison to that resulting from direct fluid injection due to the accumulation in damage from multiple heating-quenching cycles.

These results focused on the effect of heating-quenching cycles during hydraulic shearing and fracturing. However, in the actual development of EGS reservoirs, there are many other technical risks— inclusive of the uncertainty in success of deep drilling and the impact of regional geological conditions and stress regimes (Teke and Yaşar 2018). In particular, induced earthquakes associated with hydraulic fracturing is strongly associated with reactivation of preexisting faults during geothermal extraction (An et al. 2020; Igonin et al. 2021).

5 Conclusions

This study characterized the evolution of friction, stability and permeability of fractures in granite having similar geophysical properties with the geothermal reservoir rock in the Gonghe Basin of northwestern China. In particular, we explored the impact of the number of cycles of heating and then quenching in water on the evolution of these parameters. Laboratory shear-flow experiments were conducted on hot dry rock fractures at testing conditions of a confining pressures of 3 MPa, a pore fluid pressure of 70 kPa and a temperature of 25 °C. Results show that the granite fractures exhibit high frictional strength (~0.69 to 0.72) throughout all heating-quenching cycles due to the presence of high-strength and high-brittleness mineral assemblages, such as quartz, plagioclase and microcline. With an increase in the number of heating-quenching cycles, a transition from velocity-strengthening to velocity-neutral behavior is observed and this indicates a decrease in fracture stability. In addition, this stability is partly controlled by the generation of fracture wear products and the competition between fracture compaction and shear-induced dilation. Based on microstructural observations, more intergranular and intragranular microcracks are observed to develop in the granite fracture surface with an increase in the number of heating-quenching cycles. These microcracks are mainly caused by the thermal stresses during repeated heating-quenching cycles—with this potentially enhancing the instantaneous fracture permeability for higher

numbers of heating-quenching cycles. Our results have important implications in understanding the effect of heating-quenching cycles on the stability of fractures/faults and the evolution of permeability during the extraction of geothermal energy at depth.

Acknowledgements This research is funded by the National Natural Science Foundation of China (42077247, 42107163), the China Postdoctoral Science Foundation (2021M692448, 2022T150483), and the Fundamental Research Funds for the Central Universities. DE acknowledges support from the G. Albert Shoemaker endowment. We appreciate the assistance of Lei Wang in lab.

Author contributions LC, FZ and MA contributed to the conception of the study. LC and MA performed the experiments and participated in the experimental data processing, analysis and manuscript writing. FZ, LZ, DE and ZZ helped reviewing the manuscript. All authors read and approved the final manuscript.

Funding National Natural Science Foundation of China, 42077247, Fengshou Zhang, 42107163, Mengke An. China Postdoctoral Science Foundation, 2021M692448, Mengke An, 2022T150483, Mengke An. Fundamental Research Funds for the Central Universities, Fengshou Zhang. G. Albert Shoemaker endowment, Derek Elsworth.

Data availability The data generated in the present study are available from the corresponding author upon reasonable request.

Declarations

Ethics approval Not applicable.

Consent to publish All authors consent to submit the paper to *Geomechanics and Geophysics for Geo-Energy and Geo-Resources*.

Competing interests The authors declare that there are no known competing financial interests or personal relationships that could have influenced the work reported herein.

Open Access This article is licensed under a Creative Commons Attribution 4.0 International License, which permits use, sharing, adaptation, distribution and reproduction in any medium or format, as long as you give appropriate credit to the original author(s) and the source, provide a link to the Creative Commons licence, and indicate if changes were made. The images or other third party material in this article are included in the article's Creative Commons licence, unless indicated otherwise in a credit line to the material. If material is not included in the article's Creative Commons licence and your intended use is not permitted by statutory regulation or exceeds the permitted use, you will need to obtain permission directly

from the copyright holder. To view a copy of this licence, visit <http://creativecommons.org/licenses/by/4.0/>.

References

- An M, Zhang F, Elsworth D, Xu Z, Chen Z, Zhang L (2020) Friction of Longmaxi shale gouges and implications for seismicity during hydraulic fracturing. *J Geophys Res Solid Earth* 125(8):66. <https://doi.org/10.1029/2020JB019885>
- An M, Zhang F, Min KB, Elsworth D, Marone C, He C (2021) The potential for low-grade metamorphism to facilitate fault instability in a geothermal reservoir. *Geophys Res Lett* 48(11):1–10. <https://doi.org/10.1029/2021GL093552>
- Atkinson GM, Eaton DW, Igonin N (2020) Developments in understanding seismicity triggered by hydraulic fracturing. *Nat Rev Earth Environ* 1(5):264–277. <https://doi.org/10.1038/s43017-020-0049-7>
- Bao X, Eaton DW (2016) Fault activation by hydraulic fracturing in western Canada. *Science* 354(6318):1406–1409. <https://doi.org/10.1126/science.aag2583>
- Barbier E (2002) Geothermal energy technology and current status: an overview. *Renew Sustain Energy Rev* 6(1–2):3–65. [https://doi.org/10.1016/S1364-0321\(02\)00002-3](https://doi.org/10.1016/S1364-0321(02)00002-3)
- Blanpied ML, Lockner DA, Byerlee JD (1995) Frictional slip of granite at hydrothermal conditions. *J Geophys Res* 100(B7):13045–13064. <https://doi.org/10.1029/95jb00862>
- Blanpied ML, Tullis TE, Weeks JD (1998) Effects of slip, slip rate, and shear heating on the friction of granite. *J Geophys Res* 103:489–511. [https://doi.org/10.1016/0043-1648\(65\)90161-4](https://doi.org/10.1016/0043-1648(65)90161-4)
- Brown D, Duchane D, Heiken G, Hriscu V (2012) Mining the earth's heat: hot dry rock geothermal energy. Springer, New York. <https://doi.org/10.1007/978-3-540-68910-2>
- Candela T, Wassing B, ter Heege J, Buijze L (2018) How earthquakes are induced. *Science* 360(6389):598–600. <https://doi.org/10.1126/science.aat2776>
- Cao WG, Yang HF, Liu CL, Li YJ, Bai H (2018) Hydrogeochemical characteristics and evolution of the aquifer systems of Gonghe Basin, northern China. *Geosci Front* 9(3):907–916. <https://doi.org/10.1016/j.gsf.2017.06.003>
- Caulk RA, Ghazanfari E, Perdrial JN, Perdrial N (2016) Experimental investigation of fracture aperture and permeability change within enhanced geothermal systems. *Geothermics* 62:12–21. <https://doi.org/10.1016/j.geothermics.2016.02.003>
- Chang KW, Yoon H, Kim YH, Lee MY (2020) Operational and geological controls of coupled poroelastic stressing and pore-pressure accumulation along faults: Induced earthquakes in Pohang, South Korea. *Sci Rep* 10(1):1–12. <https://doi.org/10.1038/s41598-020-58881-z>
- Chen S, Yang C, Wang G (2017) Evolution of thermal damage and permeability of Beishan granite. *Appl Therm Eng* 110:1533–1542. <https://doi.org/10.1016/j.applthermaleng.2016.09.075>
- Chen Y, Zhang C, Zhao Z, Zhao X (2020) Shear behavior of artificial and natural granite fractures after

- heating and water-cooling treatment. *Rock Mech Rock Eng* 53(12):5429–5449. <https://doi.org/10.1007/s00603-020-02221-0>
- Clarke H, Verdon JP, Kettlety T, Baird AF, Kendall JM (2019) Real-time imaging, forecasting, and management of human-induced seismicity at Preston new road, Lancashire, England. *Seismol Res Lett* 90(5):1902–1915. <https://doi.org/10.1785/0220190110>
- den Hartog SAM, Spiers CJ (2014) A microphysical model for fault gouge friction applied to subduction megathrusts. *J Geophys Res Solid Earth* 119:1510–1529. <https://doi.org/10.1002/2013JB010580>. Received
- Dieterich JH (1978) Time-dependent friction and the mechanics of stick-slip. *Pure Appl Geophys* 116(4–5):790–806. <https://doi.org/10.1007/BF00876539>
- Dieterich JH (1979) Modeling of rock friction 1. Experimental results and constitutive equations. *J Geophys Res Solid Earth* 84(B5):2161–2168. <https://doi.org/10.1029/JB084iB05p02161>
- Ellsworth WL (2013) Injection-induced earthquakes. *Science* 341(6142):1225942. <https://doi.org/10.1126/science.1225942>
- Elsworth D, Spiers CJ, Niemeijer AR (2016) Understanding induced seismicity. *Science* 354(6318):1380–1381. <https://doi.org/10.1126/science.aal2584>
- Fang Y, Elsworth D, Wang C, Ishibashi T, Fitts JP (2017) Frictional stability-permeability relationships for fractures in shales. *J Geophys Res Solid Earth* 122(3):1760–1776. <https://doi.org/10.1002/2016JB013435>
- Faoro I, Niemeijer A, Marone C, Elsworth D (2009) Influence of shear and deviatoric stress on the evolution of permeability in fractured rock. *J Geophys Res Solid Earth*. <https://doi.org/10.1029/2007JB005372>
- Gautam PK, Dwivedi R, Kumar A, Kumar A, Verma AK, Singh KH et al (2021) Damage characteristics of Jalore granitic rocks after thermal cycling effect for nuclear waste repository. *Rock Mech Rock Eng* 54:235–254. <https://doi.org/10.1007/s00603-020-02260-7>
- Grigoli F, Cesca S, Rinaldi AP, Manconj A, López-Comino JA, Clinton JF et al (2018) The November 2017 Mw 5.5 Pohang earthquake: a possible case of induced seismicity in South Korea. *Science* 360(6392):1003–1006. <https://doi.org/10.1126/science.aat2010>
- Igonin N, Verdon JP, Kendall JM, Eaton DW (2021) Large-scale fracture systems are permeable pathways for fault activation during hydraulic fracturing. *J Geophys Res Solid Earth* 126(3):1–19. <https://doi.org/10.1029/2020JB020311>
- Ishibashi T, Watanabe N, Hirano N, Okamoto A, Tsuchiya N (2014) Beyond-laboratory-scale prediction for channeling flows through subsurface rock fractures with heterogeneous aperture distributions revealed by laboratory evaluation. *J Geophys Res Solid Earth* 120:106–124. <https://doi.org/10.1002/2014JB011555>
- Ishibashi T, Elsworth D, Fang Y, Riviere J, Madara B, Asanuma H et al (2018) Friction-stability-permeability evolution of a fracture in granite. *Water Resour Res* 54(12):9901–9918. <https://doi.org/10.1029/2018WR022598>
- Jiang G, Zuo J, Li L, Ma T, Wei X (2018) The evolution of cracks in maluanshan granite subjected to different temperature processing. *Rock Mech Rock Eng* 51(6):1683–1695. <https://doi.org/10.1007/s00603-018-1403-7>
- Kant MA, Ammann J, Rossi E, Madonna C, Höser D, Rudolf von Rohr P (2017) Thermal properties of Central Aare granite for temperatures up to 500°C: irreversible changes due to thermal crack formation. *Geophys Res Lett* 44(2):771–776. <https://doi.org/10.1002/2016GL070990>
- Kumari WGP, Ranjith PG, Perera MSA, Chen BK, Abdulagatov IM (2017) Temperature-dependent mechanical behaviour of Australian Strathbogie granite with different cooling treatments. *Eng Geol* 229:31–44. <https://doi.org/10.1016/j.enggeo.2017.09.012>
- Lee K-K, Ellsworth WL, Giardini D, Townend J, Ge S, Shimamoto T et al (2019) Managing injection-induced seismic risks. *Science* 364(6442):730–732. <https://doi.org/10.1126/science.aax1878>
- Lei X, Wang Z, Su J (2019a) Possible link between long-term and short-term water injections and earthquakes in salt mine and shale gas site in Changning, south Sichuan Basin, China. *Earth Planet Phys* 3(6):510–525. <https://doi.org/10.26464/epp2019052>
- Lei X, Wang Z, Su J (2019b) The December 2018 ML 5.7 and January 2019b mL 5.3 earthquakes in South Sichuan basin induced by shale gas hydraulic fracturing. *Seismol Res Lett* 90(3):1099–1110. <https://doi.org/10.1785/0220190029>
- Li N, Wang HB, Zhang SC, Zou YS, Zhang ZP, Zhou T (2021) Effect of cyclic thermal shock on mechanical properties and brittleness of granite. In: 55th U.S. rock mechanics/geomechanics symposium 2021, vol 3, pp 286–292. <https://doi.org/10.2113/2021/4296301/5366964/4296301.pdf>
- Majer EL, Baria R, Stark M, Oates S, Bommer J, Smith B, Asanuma H (2007) Induced seismicity associated with enhanced geothermal systems. *Geothermics* 36(3):185–222. <https://doi.org/10.1016/j.geothermics.2007.03.003>
- Marone C (1998) Laboratory-derived friction laws and their application to seismic faulting. *Annu Rev Earth Planet Sci* 26:643–696. <https://doi.org/10.1146/annurev.earth.26.1.643>
- Mitchell TM, Faulkner DR (2008) Experimental measurements of permeability evolution during triaxial compression of initially intact crystalline rocks and implications for fluid flow in fault zones. *J Geophys Res Solid Earth*. <https://doi.org/10.1029/2008JB005588>
- Mo C, Zhao J, Zhang D (2022) Real-time measurement of mechanical behavior of granite during heating-cooling cycle: a mineralogical perspective. *Rock Mech Rock Eng* 55(7):4403–4422. <https://doi.org/10.1007/s00603-022-02867-y>
- Moore DE, Lockner DA (2011) Frictional strengths of talc-serpentine and talc-quartz mixtures. *J Geophys Res* 116:B01403. <https://doi.org/10.1029/2010JB007881>
- Moore DE, Lockner DA, Byerlee JD (1994) Reduction of permeability in granite at elevated temperatures. *Science* 265:1558–1561. <https://doi.org/10.1126/science.265.5178.1558>
- Morrow CA, Moore DE, Lockner DA (2001) Permeability reduction in granite under hydrothermal conditions.

- J Geophys Res Solid Earth 106(B12):30551–30560. <https://doi.org/10.1029/2000JB000010>
- Moya D, Aldás C, Kaparaju P (2018) Geothermal energy: Power plant technology and direct heat applications. *Renew Sustain Energy Rev* 94:889–901. <https://doi.org/10.1016/j.rser.2018.06.047>
- Okamoto A, Tanaka H, Watanabe N, Saishu H, Tsuchiya N (2017) Fluid pocket generation in response to heterogeneous reactivity of a rock fracture under hydrothermal conditions. *Geophys Res Lett* 44:10306–10315. <https://doi.org/10.1002/2017GL075476>
- Passelègue FX, Spagnuolo E, Violay M, Nielsen S, Di Toro G, Schubnel A (2016) Frictional evolution, acoustic emissions activity, and off-fault damage in simulated faults sheared at seismic slip rates. *J Geophys Res Solid Earth* 121:7490–7513. <https://doi.org/10.1002/2016JB012988>
- Peng H, Zhao Z, Chen W, Chen Y, Fang J, Li B (2020) Thermal effect on permeability in a single granite fracture: experiment and theoretical model. *Int J Rock Mech Min Sci* 131:104–358. <https://doi.org/10.1016/j.ijrmmms.2020.104358>
- Reinsch T, Dobson P, Asanuma H, Huenges E, Poletto F, Sanjuan B (2017) Utilizing supercritical geothermal systems: a review of past ventures and ongoing research activities. *Geotherm Energy*. <https://doi.org/10.1186/s40517-017-0075-y>
- Ruina A (1983) Slip instability and state variable friction laws. *J Geophys Res* 88(B12):10359–10370. <https://doi.org/10.1029/JB088iB12p10359>
- Shimizu I (1995) Kinetics of pressure solution creep in quartz: theoretical considerations. *Tectonophysics* 245:121–134. [https://doi.org/10.1016/0040-1951\(94\)00230-7](https://doi.org/10.1016/0040-1951(94)00230-7)
- Singh HK, Sinha SK, Chandrasekharam D (2020) A preliminary investigation for the assessment of geothermal potential at Eastern Peninsular India. *Geomech Geophys Geo-Energy Geo-Resour* 6:9. <https://doi.org/10.1007/s40948-019-00133-0>
- Sun C, Zhuang L, Jung S, Lee J, Yoon JS (2021) Thermally induced slip of a single sawcut granite fracture under biaxial loading. *Geomech Geophys Geo-Energy Geo-Resour* 7(4):1–13. <https://doi.org/10.1007/s40948-021-00293-y>
- Tang ZC, Peng MH, Xiao S (2022) Basic friction angle of granite fracture after heating and rapid cooling treatments. *Eng Geol*. <https://doi.org/10.1016/j.enggeo.2022.106626>
- Tanikawa W, Sakaguchi M, Tadai O, Hirose T (2010) Influence of fault slip rate on shear-induced permeability. *J Geophys Res Solid Earth*. <https://doi.org/10.1029/2009JB007013>
- Tanikawa W, Tadai O, Mukoyoshi H (2014) Permeability changes in simulated granite faults during and after frictional sliding. *Geofluids* 14:481–494. <https://doi.org/10.1111/gfl.12091>
- Teke O, Yaşar E (2018) Geothermal energy and integrated resource management in Turkey. *Geomech Geophys Geo-Energy Geo-Resour* 4:1–10. <https://doi.org/10.1007/s40948-017-0070-6>
- Tembe S, Lockner DA, Wong T-F (2010) Effect of clay content and mineralogy on frictional sliding behavior of simulated gouges: binary and ternary mixtures of quartz, illite, and montmorillonite. *J Geophys Res* 115:B03416. <https://doi.org/10.1029/2009JB006383>
- Verdon JP, Bommer JJ (2021) Green, yellow, red, or out of the blue? An assessment of Traffic Light Schemes to mitigate the impact of hydraulic fracturing-induced seismicity. *J Seismology* 25(1):301–326. <https://doi.org/10.1007/s10950-020-09966-9>
- Wan Z, Zhao Y, Kang J (2005) Forecast and evaluation of hot dry rock geothermal resource in China. *Renew Energy* 30(12):1831–1846. <https://doi.org/10.1016/j.renene.2005.01.016>
- Wang F, Konietzky H (2022) Thermal cracking in granite during a heating-cooling cycle up to 1000 °C: laboratory testing and real-time simulation. *Rock Mech Rock Eng* 55:1411–1428. <https://doi.org/10.1007/s00603-021-02740-4>
- Wang F, Frühwirt T, Konietzky H (2020) Influence of repeated heating on physical–mechanical properties and damage evolution of granite. *Int J Rock Mech Min Sci* 136:104–514. <https://doi.org/10.1016/j.ijrmmms.2020.104514>
- Watanabe N, Numakura T, Sakaguchi K, Saishu H, Okamoto A, Ingebritsen SE et al (2017a) Potentially exploitable supercritical geothermal resources in the ductile crust. *Nat Geosci* 10:140–144. <https://doi.org/10.1038/ngeo2879>
- Watanabe N, Egawa M, Sakaguchi K, Ishibashi T, Tsuchiya N (2017b) Hydraulic fracturing and permeability enhancement in granite from subcritical/brittle to supercritical/ductile conditions. *Geophys Res Lett* 44:5468–5475. <https://doi.org/10.1002/2017GL073898>
- Watanabe N, Sakaguchi K, Goto R, Miura T, Yamane K, Ishibashi T et al (2019) Cloud-fracture networks as a means of accessing superhot geothermal energy. *Sci Rep* 9:1–11. <https://doi.org/10.1038/s41598-018-37634-z>
- Watanabe N, Saito K, Okamoto A, Nakamura K, Ishibashi T, Saishu H et al (2020) Stabilizing and enhancing permeability for sustainable and profitable energy extraction from superhot geothermal environments. *Appl Energy* 260:114306. <https://doi.org/10.1016/j.apenergy.2019.114306>
- Weng L, Wu Z, Liu Q (2020) Influence of heating/cooling cycles on the micro/macroc cracking characteristics of Rucheng granite under unconfined compression. *Bull Eng Geol Env* 79(3):1289–1309. <https://doi.org/10.1007/s10064-019-01638-4>
- White M, Fu P, McClure M, Danko G, Elsworth D, Sonnenthal E et al (2018) A suite of benchmark and challenge problems for enhanced geothermal systems. *Geomech Geophys Geo-Energy Geo-Resour* 4:79–117. <https://doi.org/10.1007/s40948-017-0076-0>
- Wood WW (2009) Guest Editorial: enhanced geothermal systems: an opportunity for hydrogeology. *Ground Water* 47(6):751. <https://doi.org/10.1111/j.1745-6584.2009.00573.x>
- Yang J, Fu LY, Wang F, Deng W (2022) Coupled thermo-mechanical damage evolution of granite under repeated heating-cooling cycles and the applications of Mohr–Coulomb and Drucker–Prager Models. *Nat Resour Res* 31(5):2629–2652. <https://doi.org/10.1007/s11053-022-10084-1>
- Yasuhara H, Elsworth D (2004) Evolution of permeability in a natural fracture: significant role of pressure solution. *J Geophys Res*. <https://doi.org/10.1029/2003jb002663>

- Yasuhara H, Elsworth D, Polak A, Liu J, Grader A, Halleck P (2006) Spontaneous switching between permeability enhancement and degradation in fractures in carbonate: lumped parameter representation of mechanically- and chemically-mediated dissolution. *Transp Porous Media* 65:385–409. <https://doi.org/10.1007/s11242-006-6386-2>
- Yasuhara H, Kinoshita N, Ohfuji H, Lee DS, Nakashima S, Kishida K (2011) Temporal alteration of fracture permeability in granite under hydrothermal conditions and its interpretation by coupled chemo-mechanical model. *Appl Geochem* 26:2074–2088. <https://doi.org/10.1016/j.apgeochem.2011.07.005>
- Yin Q, Wu J, Jiang Z, Zhu C, Su H, Jing H, Gu X (2022) Investigating the effect of water quenching cycles on mechanical behaviors for granites after conventional triaxial compression. *Geomech Geophys Geo-Energy Geo-Resour* 8:66. <https://doi.org/10.1007/s40948-022-00388-0>
- Zhang S, Tullis TE, Scruggs VJ (1999) Permeability anisotropy and pressure dependency of permeability in experimentally sheared gouge materials. *J Struct Geol* 21:795–806. [https://doi.org/10.1016/S0191-8141\(99\)00080-2](https://doi.org/10.1016/S0191-8141(99)00080-2)
- Zhang C, Jiang G, Shi Y, Wang Z, Wang Y, Li S et al (2018) Terrestrial heat flow and crustal thermal structure of the Gonghe-Guide area, northeastern Qinghai–Tibetan plateau. *Geothermics* 72:182–192. <https://doi.org/10.1016/j.geothermics.2017.11.011>
- Zhao J, Brown ET (1992) Hydro-thermo-mechanical properties of joints in the Carnmenellis granite. *Q J Eng Geol* 25(4):279–290. <https://doi.org/10.1144/gsl.qjeg.1992.025.04.03>
- Zhao X, Zeng Z, Huai N, Wang K (2020a) Geophysical responses and possible geothermal mechanism in the Gonghe Basin, China. *Geomech Geophys Geo-Energy Geo-Resour* 6:17. <https://doi.org/10.1007/s40948-020-00141-5>
- Zhao Z, Xu H, Wang J, Zhao X, Cai M, Yang Q (2020) Auxetic behavior of Beishan granite after thermal treatment: a microcracking perspective. *Eng Fract Mech* 231:107017. <https://doi.org/10.1016/j.engfracmech.2020.107017>
- Zhao Z, Hu Y, Jin P, Xu Y, Hu Y, Li C, Meng Q (2021) Experimental study on the physico-mechanical properties and temperature field evolution of granite subjected to different heating–cooling treatments. *Bull Eng Geol Env* 80(11):8745–8763. <https://doi.org/10.1007/s10064-021-02466-1>
- Zhong Z, Elsworth D, Hu Y (2016) Evolution of strength and permeability in stressed fractures with fluid–rock interactions. *Pure Appl Geophys* 173(2):525–536. <https://doi.org/10.1007/s00024-015-1099-5>
- Zhu J, Hu K, Lu X, Huang X, Liu K, Wu X (2015) A review of geothermal energy resources, development, and applications in China: current status and prospects. *Energy* 93:466–483. <https://doi.org/10.1016/j.energy.2015.08.098>

Publisher's Note Springer Nature remains neutral with regard to jurisdictional claims in published maps and institutional affiliations.